

# Improving probabilistic error cancellation in the presence of non-stationary noise

Samudra Dasgupta<sup>1,2\*</sup> and Travis S. Humble<sup>1,2†</sup>

<sup>1</sup>Quantum Science Center, Oak Ridge National Laboratory, Oak Ridge, Tennessee, USA

<sup>2</sup>Bredesen Center, University of Tennessee, Knoxville, USA

**Abstract**—We investigate the stability of probabilistic error cancellation (PEC) outcomes in the presence of non-stationary noise, which is an obstacle to achieving accurate observable estimates. Leveraging Bayesian methods, we design a strategy to enhance PEC stability and accuracy. Our experiments using a 5-qubit implementation of the Bernstein-Vazirani algorithm and conducted on the `ibm_kolkata` device reveal a 42% improvement in accuracy and a 60% enhancement in stability compared to non-adaptive PEC. These results underscore the importance of adaptive estimation processes to effectively address non-stationary noise, vital for advancing PEC utility.

**Index Terms**—Stability, probabilistic error cancellation, non-stationary quantum channels, Bayesian inference

## I. INTRODUCTION

Error-resilient quantum computing holds great promise, offering significant advancements over conventional computing. Once realized, it is expected to super-polynomially reduce execution time, energy consumption, and memory storage needs compared to conventional state-of-the-art computers [1]. The potential impact of error-resilient quantum computing includes revolutionizing scientific applications such as simulating many-body quantum systems [2], solving large-scale optimization problems [3], efficiently sampling high-dimensional probability distributions [4], factorizing large integers, and enhancing the security of communication networks [5]. Consequently, this technology is expected to be disruptive to sectors such as telecommunications, cyber-security, pharmaceuticals, logistics, supply chain management, artificial intelligence, and materials science [6].

The practical realization of quantum computing has witnessed rapid advancements [7], with quantum devices now operating as systems with hundreds of interacting qubits. However, these real quantum devices [8] are noisy [9], and practical efforts to realize a quantum computer introduce various noise processes like decay, de-coherence [10], environmental coupling, intra-register cross-talk [11, 12], and leakage from computational

space [13]. Physical operations like quantum gates and measurements rely on electromagnetic fields susceptible to pulse distortion, attenuation, jitter, and drift, which further increase noise [14, 15]. Imperfections in thermodynamic controls (such as cryogenic cooling, magnetic shielding, vibration suppression, and imperfect vacuum chambers) can disturb the operating conditions of the quantum computer [16, 17].

These lead to computational errors that make it essential to address noise and implement error mitigation strategies [18] to improve the accuracy of quantum outcome [19].

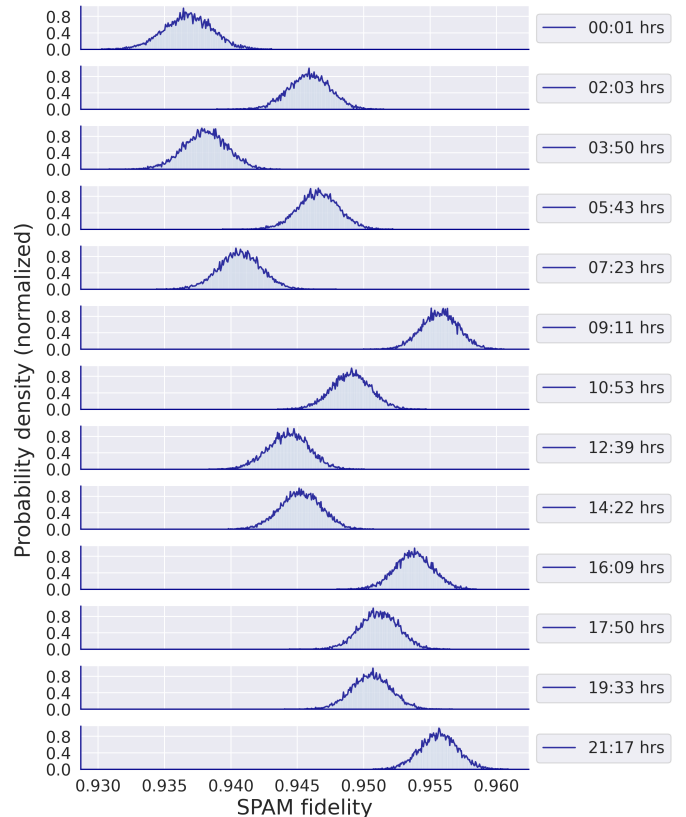


**Figure 1:** Non-stationary distribution functions of the state preparation and measurement (SPAM) fidelity for qubit 2 on `ibm_kolkata` superconducting device collected on Jan 15, 2024.

Contemporary quantum computers are not only noisy but they also exhibit non-stationarity. Non-stationary noise pro-

This manuscript has been authored by UT-Battelle, LLC under Contract No. DE-AC05-00OR22725 with the U.S. Department of Energy. The United States Government retains and the publisher, by accepting the article for publication, acknowledges that the United States Government retains a non-exclusive, paid-up, irrevocable, worldwide license to publish or reproduce the published form of this manuscript, or allow others to do so, for United States Government purposes. The Department of Energy will provide public access to these results of federally sponsored research in accordance with the DOE Public Access Plan (<https://www.energy.gov/doe-public-access-plan>).

cesses [20, 21, 22, 23, 24] in superconducting qubits [25] are well-studied. For example, state preparation and measurement (SPAM) fidelities have been observed to fluctuate significantly, showing more than 25% deviation from their long-term average [26]. Similarly, the fidelity of CNOT gates have been noted to change by over 40% within similar time frames [27]. Moreover, the qubit relaxation time ( $T_1$ ) has been observed to experience fluctuations of up to 400% in just 30 minutes [28]. Likewise, de-phasing time ( $T_2$ ) has been recorded to vary by over 50% within an hour [29, 30].

The non-stationarity observed in contemporary superconducting quantum computers stems from two primary sources linked to material defects: impurities within the material and ionization induced by cosmic rays. It is theorized that fluctuating two-level systems, possibly stemming from certain oxides on the superconductor’s surface, contribute to non-stationarity [23, 24]. Additionally, cosmic rays [31, 21] contribute by ionizing the substrate upon impact, leading to the emission of high-energy phonons, which in turn triggers a burst of quasi-particles. These quasi-particles disrupt qubit coherence across the device. It has been shown that quantum computers can experience catastrophic errors in multi-qubit registers approximately every 10 seconds due to cosmic rays originating from outer space [21]. Studies that address non-stationary noise in superconducting quantum computers include investigations on output reproducibility [32], noise modeling [22], tracking the non-stationary profile of quantum noise [33], and quantum error mitigation using continuous control [34].

Quantum error mitigation is a set of techniques that employs statistical tools from estimation theory to reduce the impact of noise in quantum computations without directly correcting the quantum state [18]. Such techniques can become vulnerable to errors stemming from over or under estimation of noise due to the presence of non-stationarity [35, 36].

A quantum noise channel [37] can be described as a stochastic process, allowing for the continuous update of its estimated characteristics in response to varying noise conditions. Such an approach treats the channel as a time-varying random variable. Consider Fig. 1 which shows the state preparation and measurement (SPAM) fidelity for the second register element on `ibm_kolkata` device on Jan 15, 2024. The probability density is clearly changing with time, even though the variance stays consistent. In light of such non-stationary data, a single-qubit SPAM noise channel can be described by the model:  $\mathcal{E}(\rho) = f(t)\rho + [1 - f(t)]\mathbb{X}\rho\mathbb{X}$ , where  $\rho$  represents the single-qubit density matrix,  $\mathbb{X} = \begin{pmatrix} 0 & 1 \\ 1 & 0 \end{pmatrix}$  denotes the Pauli-X matrix, and  $f(t)$  denotes the SPAM fidelity drawn from a time-dependent distribution. From Fig. 1, non-stationarity of noise in this superconducting device is apparent within 24 hours. The noise parameters estimated during device re-calibration quickly becomes outdated, compromising the accuracy of noise channel information essential for mitigation. Thus re-calibration alone is insufficient and there is a need for adaptive error mitigation

techniques that can function in between calibration intervals in the face of changing noise conditions.

This study focuses on probabilistic error cancellation (PEC) [38] in the presence of non-stationary noise. PEC is a quantum error mitigation approach that aims to construct unbiased estimates of the means of quantum observables from noisy observations. Effective implementation requires an accurate noise characterization [39]. For example, learning correlated noise channels in large quantum circuits on a superconducting quantum processor has proven to be difficult [40]. Yet, leveraging sparse noise models, PEC has been successful in estimating the mean of observables in circuits comprising 2,880 CNOT gates, executed on a 127-qubit noisy superconducting processor - a task that conventional brute-force computing could not match [41].

We demonstrate that adaptive probabilistic error cancellation, which views quantum noise channels as evolving random variables, outperforms its non-adaptive counterpart in devices subject to non-stationary noise. To achieve this aim, we will make use of a 5-qubit implementation of the Bernstein-Vazirani algorithm [42].

The manuscript is organized as follows. In Sec. II, we provide background for probabilistic error cancellation (PEC). Sec. III develops a Bayesian [43, 44] approach for adapting the method of probabilistic error cancellation to non-stationary noise. It also sets up a performance evaluation framework for the accuracy and stability of PEC results. Sec. IV presents a numerical validation of adaptive probabilistic error cancellation using a 5-qubit implementation of the Bernstein-Vazirani algorithm, where we treat the noise parameters (qubit-specific state preparation and measurement (SPAM) fidelities and depolarizing parameters characterizing noise in CNOT gate) as non-stationary random variables. In Sec. V, we present the results of experiments conducted on a real, noisy quantum device to test the adaptive PEC algorithm. Concluding remarks are provided in Sec. VI.

## II. BACKGROUND

In this section, we provide background for the quantum error mitigation method called probabilistic error cancellation (PEC) [38, 40, 41] which aims to mitigate errors by approximating the noiseless mean of the observable as a weighted sum of noisy observables. We use calligraphic symbols to denote super-operators acting on density matrices ( $\rho$ ):

$$\mathcal{G}\rho = G\rho G^\dagger. \quad (1)$$

where  $\mathcal{G}$  is the super-operator and  $G$  is a unitary quantum operator. For example, if  $G$  denotes the CNOT operator, then  $\mathcal{G}$  is the super-operator for the CNOT operation.

Typically we do not have access to a noiseless implementation of  $\mathcal{G}$ . Let  $\tilde{\mathcal{G}}$  denote the super-operator corresponding to the available, noisy implementation of  $\mathcal{G}$ . We have access to other synthesized implementations of  $\tilde{\mathcal{G}}$  by subjecting  $\tilde{\mathcal{G}}$  to basis operations available on a noisy device. Originally, the noisy

basis set was specified as the set of native gates that a quantum computer could implement [38]. However, with advancements in superconducting quantum computers, the noise associated with single-qubit Pauli operators has become negligible [40, 45]. Consequently, Pauli operators, which might be a composition of multiple native gates, can be employed as the basis set [46]. We denote by  $\{\tilde{\mathcal{G}}_k\}$  the set of all noisy super-operators, with  $k=0$  denoting the noisy implementation of  $\mathcal{G}$  without additional operations from the basis set.

As an example, consider a 2-qubit quantum gate  $G$ . The set of noisy super-operators composed under a Pauli channel assumption are given by:  $\{\mathcal{P} \circ \tilde{\mathcal{G}}\}$  where  $\mathcal{P} \circ \tilde{\mathcal{G}}(\rho) = \mathcal{P}(\tilde{\mathcal{G}}(\rho))$  and  $\mathcal{P}(\cdot) \equiv [\mathbb{P}_0 \otimes \mathbb{P}_1](\cdot)[\mathbb{P}_0 \otimes \mathbb{P}_1]$ . Here 0 and 1 refer to qubit 0 and qubit 1 respectively and  $\mathbb{P}_0, \mathbb{P}_1$  are picked from the set of Pauli operators  $\{\mathbb{I}, \mathbb{X}, \mathbb{Y}, \mathbb{Z}\}$ . Thus, by varying  $P_0$  and  $P_1$ , we obtain the set  $\{\mathcal{P} \circ \tilde{\mathcal{G}}\}$  which forms a basis  $\{\tilde{\mathcal{G}}_k\}_{k=0}^{15}$  that spans the super-operator space. In this 2-qubit example, the map for  $k$  is derived from the Cartesian product of  $\{\mathbb{I}, \mathbb{X}, \mathbb{Y}, \mathbb{Z}\} \times \{\mathbb{I}, \mathbb{X}, \mathbb{Y}, \mathbb{Z}\}$ , with the sequence of this ordered set determining the value of  $k$ .

In general, the super-operator  $\mathcal{G}$  can be expressed as a linear combination of the basis super-operators:

$$\mathcal{G} = \sum_{k=0}^{N_p-1} \eta_k \tilde{\mathcal{G}}_k, \quad (2)$$

where  $N_p$  is the dimension of the super-operator space. The PEC coefficients  $\eta_k$  in the linear combination are determined either analytically, under a noise model assumption for single and two-qubit gates, which can be extended to larger circuits, or numerically, by minimizing the one-norm between high-dimensional matrices [46, 38]. We employ the analytical approach.

The circuits corresponding to the super-operators  $\tilde{\mathcal{G}}_k$  in Eqn. 2 are constructed by subjecting each of the gates in the quantum circuit for  $\mathcal{G}$  to operations from the noisy basis set. If we execute these noisy circuits and collect the mean of the observable, then, from Eqn. 2, we recover the ideal noiseless mean of an observable  $\langle \mathcal{O} \rangle$  as:

$$\langle \mathcal{O} \rangle = \text{Tr}[\mathcal{O}\mathcal{G}\rho] = \text{Tr}\left[\mathcal{O} \sum_k \eta_k \tilde{\mathcal{G}}_k \rho\right] \quad (3)$$

where  $\rho$  is the input density matrix to the circuit. Thus, an observable  $\langle \mathcal{O} \rangle$  may be estimated as a weighted sum of the mean of the observables from the noisy circuits.

Eqn. 3 can be re-written as:

$$\langle \mathcal{O} \rangle = \gamma \sum_k \text{sgn}(\eta_k) \mathbb{Q}_k \text{Tr}\left[\mathcal{O}\tilde{\mathcal{G}}_k \rho\right] \quad (4)$$

with  $\gamma = \sum |\eta_k|$  and  $\mathbb{Q}_k = |\eta_k|/\gamma$ . The sign function,  $\text{sgn}(\cdot)$ , returns +1 for positive inputs, -1 for negative inputs, and 0 for an input of 0.

Note that the set  $\{\mathbb{Q}_k\}$  forms a valid probability distribution because all its elements are positive and sum to 1. However,

$\{\mathbb{Q}_k\}$  is termed a quasi-probability distribution (QPD) [38, 46]. To see this, consider a random integer  $K \in \{0, \dots, N_p - 1\}$  which follows the probability distribution function denoted by  $\mathbb{Q}_k$ . This random integer  $K$  can be mapped one-to-one to the random variable  $\text{sgn}(\eta_k) \text{Tr}\left[\mathcal{O}\tilde{\mathcal{G}}_k \rho\right]$ , which inherits the probability distribution function  $\mathbb{Q}_k$ . By repeatedly sampling the random variable  $K$ , we realize a set of random integers represented as  $\{m\}$ . For each specific  $m$  that is realized, we execute the corresponding noisy quantum circuit  $\tilde{\mathcal{G}}_m$  multiple times and obtain a set of noisy means of observables denoted by the set  $\left\{\text{Tr}\left[\mathcal{O}\tilde{\mathcal{G}}_m \rho\right]\right\}$ .

When computing the average over the set of noisy means of observables  $\left\{\text{Tr}\left[\mathcal{O}\tilde{\mathcal{G}}_m \rho\right]\right\}$ , we need to adjust the sign of each element of the set by the sign of  $\eta_m$  and scale it by  $\gamma$ . This average then converges to the mean of the observable from a noiseless gate  $\mathcal{G}$ , in the asymptotic limit of a large number of repeated samplings of the random variable  $K$ . The need for adjustment by the sign function leads us to denote  $\mathbb{Q}_k$  as quasi-probabilities.

Achieving an accuracy of  $O(\epsilon)$  using the empirical mean of the random variable  $\gamma \text{sgn}(\eta_k) \text{Tr}\left[\mathcal{O}\tilde{\mathcal{G}}_k \rho\right]$  (which is an unbiased estimator of  $\langle \mathcal{O} \rangle$ ) requires  $O(\gamma/\epsilon)^2$  PEC circuit samples and the result has variance of order  $O(\gamma^2)$  [38].

### III. ADAPTIVE PEC

Estimating channel noise parameters is crucial for determining the PEC coefficients  $\{\eta_k\}$ . However, the non-stationary nature of noise, along with drift and latency in characterization, complicates this task. This in turn makes it difficult to accurately assess the PEC coefficients. In this section, we demonstrate how adaptive parameter estimation can be applied to PEC.

The parameters characterizing the noise during idle time (such as qubit decoherence time [47]) and quantum operations (such as CNOT fidelity [26]) exhibit random non-stationary behavior in some hardware. Estimating non-stationary stochastic processes is challenging and their predictive value is limited because the patterns identified from historical data may not reliably indicate future behavior, making it difficult to discern underlying trends. A model that is effective at one time point can become inaccurate at another.

However, we can utilize intermittent incremental measurements from quantum circuits to devise a Bayesian [43, 44, 48, 49] update for the current state of the device noise:

$$\Pr(\mathbf{x}|\text{data}) \propto \Pr(\text{data}|\mathbf{x}) \Pr(\mathbf{x}) \quad (5)$$

where data refers to measurements obtained from circuit execution,  $\mathbf{x}$  denotes the multi-dimensional vector of parameters characterizing the device noise (such as connection-specific CNOT fidelity and qubit-specific SPAM fidelities),  $\Pr(\mathbf{x}|\text{data})$  is the posterior noise distribution,  $\Pr(\text{data}|\mathbf{x})$  is the likelihood, and  $\Pr(\mathbf{x})$  is the prior noise distribution. We use this to update  $\{\eta_k\}$  via updates to model-specific parameters.

Obtaining the posterior distribution for  $x$  is a two-step process: first, we estimate the posterior for uncorrelated parameters, and second, for correlated parameters in the underlying noise model.

### A. Uncorrelated parameters

Uncorrelated parameters refer to those model parameters for which there exist datasets (such as the partial trace of the observable on a single qubit) where the observed data is modeled by error due to only one noise parameter. Here, the analysis is simpler as univariate priors can be used. For example, if we disregard noise from single-qubit rotations, then the measurements obtained from any qubit that was not subjected to entangling operations, can be described by a one-parameter model under symmetric SPAM noise model.

Let  $\mathcal{D}_q = \{b_q(0), \dots, b_q(L-1)\}$  represent a dataset of  $L$  samples obtained for qubit  $q$  after measurement in the computational basis. Each  $b_q(l)$  is a single-bit measured after the  $l$ -th execution of  $\tilde{\mathcal{G}}_0$ . We can adopt a beta distribution as the prior for the SPAM fidelity  $f_q$  because the beta distribution is well-suited for values restricted to the  $[0,1]$  interval and can effectively accommodate the experimentally observed unimodal and skewed density as seen in Fig. 1. The beta distribution's flexibility allows for an accurate fit to these characteristics. The Beta distribution with parameters  $\alpha_q, \beta_q$  is given by  $\text{Beta}(f_q; \alpha_q, \beta_q) = f_q^{\alpha_q-1} (1-f_q)^{\beta_q-1} / B(\alpha_q, \beta_q)$  where the normalizing denominator  $B(\alpha_q, \beta_q)$  is the Beta function defined as  $B(m, n) = \Gamma(m)\Gamma(n)/\Gamma(m+n)$ , and  $\Gamma(\cdot)$  is the gamma function  $\Gamma(y) = \int_0^\infty t^{y-1} e^{-t} dt$ , defined for any positive  $y$ .

The prior for the mean  $\mu_q^{\text{prior}}$  and variance  $v_q^{\text{prior}}$  of the SPAM fidelity  $f_q$  can be derived from historical characterization data (e.g. using data post calibration). If such data is not accessible, we can obtain the starting point from a small perturbation to the ideal value. The prior parameters are then obtained as:  $\alpha_q^{\text{prior}} = \mu_q^{\text{prior}} \left[ \mu_q^{\text{prior}} (1 - \mu_q^{\text{prior}}) / v_q^{\text{prior}} - 1 \right]$  and  $\beta_q^{\text{prior}} = (1 - \mu_q^{\text{prior}}) \left[ \mu_q^{\text{prior}} (1 - \mu_q^{\text{prior}}) / v_q^{\text{prior}} - 1 \right]$ .

The likelihood is obtained as:

$$\mathcal{L}(f_q) = f_q^{C_0[\mathcal{D}_q]} (1-f_q)^{L-C_0[\mathcal{D}_q]} / B^L(\alpha_q, \beta_q) \quad (6)$$

where  $C_0[\mathcal{D}_q]$  counts the number of 0's in the dataset  $\mathcal{D}_q$ . The updated posterior density (indicated by the prime on the updated parameters) for the SPAM fidelity ( $f_q$ ) [50]:

$$f_q | \mathcal{D}_q \sim \text{Beta}(\alpha'_q, \beta'_q) \quad (7)$$

where  $\alpha'_q = \alpha_q + L - C_0[\mathcal{D}_q]$  and  $\beta'_q = \beta_q + C_0[\mathcal{D}_q]$ . This shows the influence of incremental measurements on posterior noise density. The qubit-wise updated mean [51] of the SPAM fidelity, obtained as  $\mu'_q = \alpha'_q / (\alpha'_q + \beta'_q)$ , are then used in estimating the PEC coefficients.

### B. Correlated parameters

The second task involves the adaptive estimation of correlated noise parameters, which is more complex due to the measurements being influenced by multiple noise processes simultaneously. These are the noise parameters for which there exist datasets (typically the partial trace of an observable across a subset of qubits) which reflect errors from various noise parameters jointly. The analysis uses the probability of observing classical bit-strings on this qubit subset as the random variables.

For a subset of  $m$  qubits from a total of  $n$  qubits, there are  $M = 2^m$  possible observed bit-strings, each with a probability denoted by  $p_0, p_1, \dots, p_{M-1}$ , where  $p_0$  represents the probability of observing all zeros and  $p_{M-1}$  that of all ones. These probabilities are treated as random variables which form a probability simplex, as they are all positive and add up to 1. Hence the natural way to model the joint density is using a Dirichlet prior given by:

$$\text{Pr}(p_0, \dots, p_{M-1}) = \frac{\Gamma(\sum a_i)}{\prod_{i=0}^{M-1} \Gamma(a_i)} \prod_{i=0}^{M-1} p_i^{a_i-1} \quad (8)$$

where the gamma function  $\Gamma(\cdot)$  was already defined previously and  $\{a_i : a_i > 0, i \in \{0, \dots, M-1\}\}$  are the parameters characterizing the Dirichlet distribution that need to be estimated and updated – a multi-variate task analogous to the uni-variate task for the beta distribution in the previous section.

We denote the dataset derived from  $L$  measurements of the  $m$  qubits in the computational basis as  $\mathcal{D} = \{w(0), \dots, w(L-1)\}$ , where each  $w(i)$  is a binary string of length  $m$ . The likelihood function is given by:

$$\mathcal{L}(p_0, \dots, p_{M-1}) = \prod_{i=0}^{M-1} p_i^{C_{v_i}[\mathcal{D}]} \quad (9)$$

where  $v_i \in \{0, 1\}^m$ ,  $C_{v_i}[\mathcal{D}]$  is the count of occurrences of the string  $v_i$  in the dataset  $\mathcal{D}$ . Note that  $w(i)$  is a specific realization post-measurement that takes one of the values in the set  $\{v_i\}$ .

The posterior joint density is also a Dirichlet distribution [52]:

$$\text{Pr}(p_0, \dots, p_{M-1} | \mathcal{D}) = \frac{\Gamma(\sum a'_i)}{\prod_{i=0}^{M-1} \Gamma(a'_i)} \prod_{i=0}^{M-1} p_i^{a'_i-1} \quad (10)$$

with parameters

$$a'_i = a_i + C_{v_i}(\mathcal{D}). \quad (11)$$

Upon marginalizing this joint density, the marginals follow a Beta distribution. For example, the random variable  $p_i$  is Beta-distributed with parameters [53]:

$$\begin{aligned} \alpha_i &= a'_i \\ \beta_i &= -a'_i + \sum_{j=0}^{M-1} a'_j \end{aligned} \quad (12)$$



The updated marginals from the Dirichlet distribution give us the evolving densities for each  $p_i$ , allowing us to calculate their time-varying means and variances. Specifically, the mean for  $p_i$  updates to:

$$\mathbb{E}(p_i) = \frac{a'_i}{\sum_j a'_j} \quad (13)$$

and its variance updates to:

$$\text{Var}(p_i) = \frac{a'_i \left( \sum_j a'_j - a'_i \right)}{\left( \sum_j a'_j \right)^2 \left( 1 + \sum_j a'_j \right)}. \quad (14)$$

At the final stage, the method employs the relationship between the probabilities  $p_0, \dots, p_{M-1}$  and the noise model parameters to derive the time-dependent parameter means and variances of the noise parameters. The process concludes by updating the quasi-probability distribution using the updated noise parameters per Eqn. 5.

### C. Accuracy and stability

We next evaluate the performance of PEC in presence of non-stationary noise using the lens of accuracy and stability. A mean of a quantum observable  $\mathcal{O}$  is represented as  $\langle \mathcal{O} \rangle_x$  (where  $x$  labels the noise instance), while the observed mean after mitigation is denoted as  $\langle \mathcal{O} \rangle_x^{\text{mit}}$ , which equals  $\langle \mathcal{O} \rangle$  only in the asymptotic limit of infinite samples and zero noise. To denote the mitigated noisy mean at a specific time  $t$ , we use  $\langle \mathcal{O} \rangle_x^{\text{mit}}(t)$ .

We say that a PEC mitigated observable is  $\epsilon$ -accurate if the absolute difference between the mitigated and noiseless observable is upper bounded by  $\epsilon$ :

$$|\langle \mathcal{O} \rangle_x^{\text{mit}} - \langle \mathcal{O} \rangle| \leq \epsilon \quad (15)$$

Now, suppose the underlying noise, being non-stationary, is characterized by a time-dependent density  $f(x; t)$ . We say that a PEC mitigated observable is  $\epsilon$ -stable between times  $t_1$  and  $t_2$  if:

$$|\langle \mathcal{O} \rangle_x^{\text{mit}}(t_1) - \langle \mathcal{O} \rangle_x^{\text{mit}}(t_2)| \leq \epsilon \quad (16)$$

where

$$\begin{aligned} \langle \mathcal{O} \rangle_x^{\text{mit}}(t) &= \int_x \langle \mathcal{O} \rangle_x^{\text{mit}} f(x; t) dx \\ &= \int_x \sum_k \eta_k(x, t) \text{Tr} \left[ \mathcal{O} \tilde{\mathcal{G}}_k \rho \right] f(x; t) dx \end{aligned} \quad (17)$$

Note the dependence of  $\eta_k$  on the random variable  $x$  and time  $t$ . When measuring  $\mathcal{O}_q$  for qubit  $q$ , the qubit-wise accuracy metric is:

$$\epsilon_q = |\langle \mathcal{O}_q \rangle_x - \langle \mathcal{O}_q \rangle| \quad (18)$$

without mitigation, and

$$\epsilon_q = \left| \langle \mathcal{O}_q \rangle_x^{\text{mit}} - \langle \mathcal{O}_q \rangle \right| \quad (19)$$

with error mitigation. The register average, for a  $n$ -qubit register, is:

$$\epsilon_R = \sum_{q=0}^{n-1} \epsilon_q / n \quad (20)$$

Similarly, the qubit-wise stability metric is:

$$s_q(t) = \left| \langle \mathcal{O}_q \rangle_x(t) - \langle \mathcal{O}_q \rangle_x(0) \right| \quad (21)$$

without mitigation, and

$$s_q(t) = \left| \langle \mathcal{O}_q \rangle_x^{\text{mit}}(t) - \langle \mathcal{O}_q \rangle_x^{\text{mit}}(0) \right| \quad (22)$$

with error mitigation. The register average, for a  $n$ -qubit register, is:

$$s_R(t) = \sum_{q=0}^{n-1} s_q(t) / n. \quad (23)$$

We expect the accuracy ( $\epsilon_q, \epsilon_R$ ) and stability ( $s_q, s_R$ ) metrics to be smaller when using adaptive PEC because of more accurate estimates for the time-varying PEC coefficients  $\{\eta_k\}$ .

## IV. NUMERICAL VALIDATION

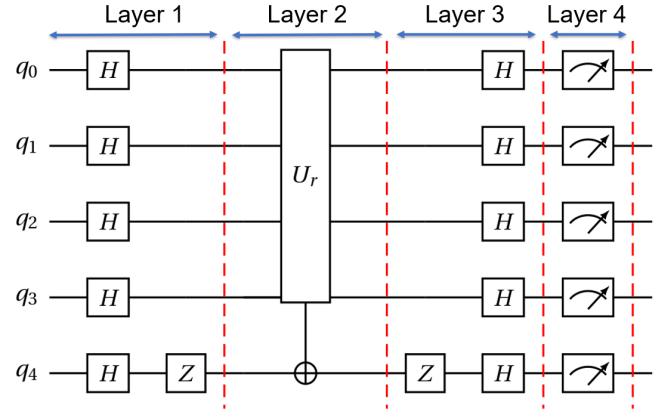


**Figure 2:** A 5-qubit implementation of the Bernstein-Vazirani algorithm with secret bit-string  $r$ .

For studying the stability and accuracy of PEC in presence of non-stationary noise, we use an implementation of the Bernstein-Vazirani algorithm [42], a standard benchmarking circuit that requires only a modest number of gates. The purpose of the algorithm is to recover a  $n$ -bit secret string  $r$ , encoded in a black-box oracle function. The algorithm identifies the secret with a single query, while the classical method needs  $2^n$  queries (worst-case).

A quantum circuit for the Bernstein-Vazirani algorithm is shown in Fig. 2. We conceptualize the circuit as having four principal layers ( $\mathbb{L}_1, \mathbb{L}_2, \mathbb{L}_3$ , and  $\mathbb{L}_4$ ) separated by dashed vertical lines. Note that the total number of qubits needed by a  $(n-1)$ -bit secret string is  $n$ , comprising  $n-1$  data qubits and one ancilla qubit. So, a 5-qubit implementation of the Bernstein-Vazirani algorithm has  $n=5$  but the secret string length is  $n-1=4$ .

The circuit is initialized with all the qubits in the register in the  $|0\rangle$  state. Thus, a pure state description yields an initial state  $|\psi_0\rangle = |0\rangle^{\otimes n}$ . In the first layer, all the qubits are subjected to Hadamard gates. The ancilla qubit (which is the last qubit with index  $n$ ) is additionally subjected to a  $\mathbb{Z}$  gate. The output after the first layer  $\mathbb{L}_1 = \mathbb{H}^{\otimes n-1} \otimes (\mathbb{Z}_n \mathbb{H}_n)$  is  $|\psi_1\rangle = |+\rangle^{\otimes n-1} |-\rangle$ .

The second layer implements the oracle function for which we can use CNOT gates. Each CNOT's control qubit corresponds to one of the bits in the secret string  $r$ , while the target qubit remains fixed at qubit  $n$ . Specifically, if the bit  $r_i$  of the secret string  $r$  is 1, we add a CNOT between qubit  $i$  (control) and qubit  $n$  (target). The input to the second layer is  $\mathbb{H}^{\otimes n-1} |0\rangle |-\rangle$  while the output is  $|\psi_2\rangle = (\mathbb{H}^{\otimes n-1} |r\rangle) |-\rangle$  where  $r$  is the secret string.

To retrieve the secret string  $r$ , the third layer requires another layer of Hadamard gates. A  $\mathbb{Z}$  gate is applied to the ancilla qubit (qubit  $n$ ) before the application of the Hadamard layer to make the computing reversible. The output quantum state after the third layer  $\mathbb{L}_3 = \mathbb{H}^{\otimes(n-1)} \otimes (\mathbb{H}_n \mathbb{Z}_n)$  is  $|\psi_3\rangle = |r\rangle |0\rangle$ .

#### A. Observable

The fourth layer is for measurement in the  $\mathbb{Z}$ -basis and is not a unitary layer. We measure the state of each of the  $n$ -qubits after projection onto the computational basis states. Post-measurement, the observation obtained is a classical bit (either 0 or 1) for each of the  $n$ -qubits measured. Thus, the final observed output is a bit-string of length  $n$ , including the ancilla.

We make a distinction between the qubit-wise observables  $\mathcal{O}_q$ , where  $q \in \{0, \dots, n\}$  and the measurement operator for the register  $M_Z = \mathbb{Z}_0 \otimes \dots \otimes \mathbb{Z}_n$  in computational basis. The qubit-wise observable  $\mathcal{O}_q$  has identity across the  $n$ -qubit tensor product except in the  $q$ -th position. For example,  $\mathcal{O}_0 = \mathbb{Z}_0 \otimes \mathbb{I}^{\otimes n-1}$  and  $\mathcal{O}_n = \mathbb{I}^{\otimes n-1} \otimes \mathbb{Z}_n$ . The eigenvalues of  $\mathcal{O}_q$  are +1 (corresponding to classical bit 0) and -1 (corresponding to classical bit 1). The theoretical mean of the qubit-wise observable  $\mathcal{O}_q$  is denoted by  $\langle \mathcal{O}_q \rangle = \text{Tr}[\mathcal{O}_q \rho]$  where  $q \in \{0, \dots, n\}$ , which reflects the measurement process being fundamentally probabilistic.

The experimentally observed mean of the observable, denoted by  $\langle \mathcal{O}_q \rangle_x$  is calculated as the sum of eigenvalues weighted by their empirically observed frequencies. In a noiseless circuit, the observed mean asymptotically converges to the theoretical mean as the sample size tends to infinity. However, in presence of shot noise and non-zero variance of  $x$ ,  $\langle \mathcal{O}_q \rangle_x$  may not equal  $\langle \mathcal{O}_q \rangle$ .

The experimentally observed measurements of the  $M_Z$  operator in computational basis belong to one of the  $2^n$  eigenstates, each of which can be represented by a  $n$ -bit binary string. These observations contain the information necessary for computing  $\mathcal{O}_q$  for all  $q$ . In the context of the Bernstein-Vazirani algorithm, we discard the ancilla bit and declare the search a success

when the first  $n$ -bits of the observed value of the  $M_Z$  operator matches the secret string  $r$ .

#### B. Modeling circuit noise

Our experimental focus is on superconducting hardware in next section. The potential sources of noise in a superconducting implementation of the circuit depicted in Fig. 2 are: (i) state preparation noise, (ii) noise in the implementation of the Hadamard gate, (iii) noise in the implementation of the  $\mathbb{Z}$  gate, (iv) noise in the implementation of the CNOT gate, and (v) measurement noise (also known as readout noise). The error resulting from the first and last noise sources, namely state preparation noise and measurement noise, are often measured collectively due to experimental limitations. This combined noise is commonly referred to as SPAM (state preparation and measurement) noise. An effective model assumes that the state preparation is noiseless, and the noise impacts the measurement (or readout) process. The relative magnitudes of the different types of noise are different. State preparation and measurement (SPAM) noise typically has the largest contribution to errors [45]. The next most significant contribution arises from imperfect implementations of entangling gates, such as the CNOT. After that the strength of the noise, for single-qubit rotations, decreases by two orders of magnitude or more [40, 45]. The  $\mathbb{Z}$  gate is a software-based operation [54] and error-free. After disregarding single-qubit rotation errors, only two predominant types of noise emerge: SPAM noise and CNOT noise.

Next, we create a quantum channel based description of the circuit noise. The circuit noise can be modeled layer-wise. The output density matrix prior to measurement can be represented as:  $\tilde{\rho} = \mathcal{E}_4(\mathcal{E}_3(\mathbb{L}_3 \mathcal{E}_2(\mathbb{L}_2 \mathcal{E}_1(\mathbb{L}_1 \rho \mathbb{L}_1^\dagger) \mathbb{L}_2^\dagger) \mathbb{L}_3^\dagger)$  where  $\mathcal{E}_k(\cdot)$  denotes the noise channel for the  $k$ -th layer of the circuit in Fig. 2. We approximate  $\mathcal{E}_1$  as identity channel because we ignore single-qubit errors.

We model noise in the CNOT gate using a 2-qubit depolarizing model. Let  $x_C(t)$  and  $x_T(t)$  represent the stochastic depolarizing parameters for the control and target qubits at time  $t$ . The depolarizing noise model for the CNOT gate is represented by:

$$\begin{aligned} \mathcal{E}_{\text{CNOT}}(\cdot) &= [1 - x_T(t)][1 - x_C(t)](\cdot) + \\ &\frac{1 - x_C(t)}{3} x_T \sum_{\mathbb{P}'_T} (\mathbb{I}_C \otimes \mathbb{P}'_T)(\cdot) (\mathbb{I}_C \otimes \mathbb{P}'_T) \\ &+ \frac{1 - x_T(t)}{3} x_C \sum_{\mathbb{P}'_C} (\mathbb{P}'_C \otimes \mathbb{I}_T)(\cdot) (\mathbb{P}'_C \otimes \mathbb{I}_T) \\ &+ \frac{x_C(t)x_T}{9} \sum_{\mathbb{P}'_C, \mathbb{P}'_T} (\mathbb{P}'_C \otimes \mathbb{P}'_T)(\cdot) (\mathbb{P}'_C \otimes \mathbb{P}'_T) \end{aligned} \quad (24)$$

In this expression, we use  $\mathbb{P}'_C, \mathbb{P}'_T \in \{\mathbb{X}, \mathbb{Y}, \mathbb{Z}\}$  as the single-qubit Pauli operators excluding identity  $\mathbb{I}$ , acting on the control (C) and target (T) qubits respectively. The sum is over all the single-qubit Pauli operators, excluding identity. Note that the effect of the quantum noise channel  $\mathcal{E}_2(\cdot)$  for layer 2, on a 5-qubit state, combines the identity channel  $\mathcal{I}$  (which acts on

qubits without CNOT connection) and  $\mathcal{E}_{\text{CNOT}}$  (which acts on qubits linked by CNOT connections).

Similar to layer 1, layer 3 also comprises single-qubit rotations only. Hence, we treat  $\mathcal{E}_3(\cdot)$  as identity channel. Lastly, the fourth layer is subjected to SPAM noise which we adapt to a noise channel description [55]. It effectively handles measurement noise by corrupting the density matrix post execution but pre measurement, and then conducting noise-free projective measurements on the corrupted output. The SPAM noise channel for qubit  $q$  has two Kraus operators  $M_0$  and  $M_1$ :

$$\begin{aligned} M_0 &= \sqrt{f_q} |0\rangle \langle 0| + \sqrt{1-f_q} |1\rangle \langle 1| \\ M_1 &= \sqrt{1-f_q} |0\rangle \langle 0| + \sqrt{f_q} |1\rangle \langle 1| \end{aligned} \quad (25)$$

where  $f_q$  represents the SPAM fidelity of qubit  $q$ . The probability of observing 0 is given by  $\text{Tr}[M_0^\dagger M_0 \rho]$  and the probability of observing 1 is given by  $\text{Tr}[M_1^\dagger M_1 \rho]$ . Note that we have assumed a symmetric model for SPAM noise with  $f_q$  denoting the average SPAM fidelities for the initial states prepared as  $|0\rangle$  and  $|1\rangle$ .

Neglecting inter-qubit cross-talk, we then have the noise channel representation for the last layer  $\mathcal{E}_4$  as a separable SPAM noise channel:

$$\mathcal{E}_4(\cdot) = \left[ \bigotimes_{q=0}^n \mathcal{E}_q^{\text{SPAM}} \right] (\cdot) \quad (26)$$

### C. PEC coefficients under Pauli noise

We first discuss CNOT noise mitigation using PEC. Following that, we discuss single-qubit SPAM noise mitigation using PEC. Then, we integrate the two discussions for noise mitigation in the quantum circuit implementation of the Bernstein-Vazirani algorithm using PEC.

1) *CNOT noise*: Let  $\tilde{\mathcal{G}}_0$  denote the super-operator for the noisy CNOT operation. Under the Pauli channel assumption, there are 16 basis super-operators, indexed by  $k$ :

$$\tilde{\mathcal{G}}_k \rho = (\mathbb{P}_C \otimes \mathbb{P}_T) \left( \tilde{\mathcal{G}}_0 \rho \right) (\mathbb{P}_C \otimes \mathbb{P}_T) \quad (27)$$

where  $\rho$  is a 2-qubit density matrix,  $\mathbb{P}_C, \mathbb{P}_T \in \{\mathbb{I}, \mathbb{X}, \mathbb{Y}, \mathbb{Z}\}$  are the single-qubit Paulis acting on the control (C) and target (T) qubits respectively, and  $k \in \{0, \dots, 15\}$ . The index  $k$  is determined by the specific combination of  $\mathbb{P}_C$  and  $\mathbb{P}_T$ , starting from  $\mathbb{I} \otimes \mathbb{I}$  for  $k = 0$  and ending with  $\mathbb{Z} \otimes \mathbb{Z}$  for  $k = 15$ , incrementing  $k$  for each subsequent combination in the sequence  $\mathbb{I}, \mathbb{X}, \mathbb{Y}, \mathbb{Z}$  applied to  $\mathbb{P}_C$  and  $\mathbb{P}_T$ .

When  $\mathbb{P}_C = \mathbb{P}_T = \mathbb{I}$ , the circuit corresponds to the noisy super-operator  $\tilde{\mathcal{G}}_0$  denoting the noisy CNOT gate available. An example of one of the remaining 15 PEC circuits for CNOT noise mitigation is shown in Fig. 3.

Using the requirement that the linear combination  $\sum \eta_k \tilde{\mathcal{G}}_k$  should equal the noiseless CNOT operation, we derive the PEC coefficients as follows. When  $\mathbb{P}_C = \mathbb{P}_T = \mathbb{I}$ ,  $\eta_0 = c_0 c_1$ . When  $\mathbb{P}_C = \mathbb{I}$  and  $\mathbb{P}_T \in \{\mathbb{X}, \mathbb{Y}, \mathbb{Z}\}$ ,  $\eta_k = c_0 x_T (1 -$

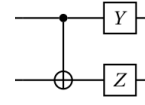


**Figure 3:** Circuit diagram for implementing one of the 16 noisy super-operators for CNOT noise mitigation using PEC. The initial noisy CNOT gate is followed up by  $\mathbb{Y}$  and  $\mathbb{Z}$  gates on the control and target qubits respectively.

$x_C)/3$ ,  $k \in \{1, 2, 3\}$ . When  $\mathbb{P}_T = \mathbb{I}$  and  $\mathbb{P}_C \in \{\mathbb{X}, \mathbb{Y}, \mathbb{Z}\}$ ,  $\eta_k = c_0 x_C (1 - x_T)/3$ ,  $k \in \{4, 8, 12\}$ . For all the remaining terms,  $\eta_k = c_0 x_C x_T / 9$ ,  $k \in \{9, 10, 11, 13, 14, 15\}$ . Here,  $c_0 = 3/[x_T(1-x_C)]^2 + [x_C(1-x_T)]^2 - 3c_1^2$  and,  $c_1 = x_C + x_T - x_C x_T - 1$ . This yields the quasi-probability distribution as:

$$\{\mathbb{Q}_k\} = \{|\eta_0|/\gamma_{\text{CNOT}}, \dots, |\eta_{15}|/\gamma_{\text{CNOT}}\} \quad (28)$$

where  $\gamma_{\text{CNOT}} = |\eta_0| + \dots + |\eta_{15}|$ .

2) *SPAM noise for qubit  $q$* : Consider a single-qubit SPAM noise channel for qubit  $q$ . The four noisy super-operators that can be implemented in this case are: (i) the SPAM noise channel:  $\tilde{\mathcal{G}}_{\mathbb{I}}(\rho) = f_q \rho + (1-f_q) \mathbb{X} \rho \mathbb{X}$ , (ii) the SPAM noise channel followed by an X error:  $\tilde{\mathcal{G}}_{\mathbb{X}}(\rho) = f_q \mathbb{X} \rho \mathbb{X} + (1-f_q) \rho$ , (iii) the SPAM noise channel followed by a Y error:  $\tilde{\mathcal{G}}_{\mathbb{Y}}(\rho) = f_q \mathbb{Y} \rho \mathbb{Y} + (1-f_q) \mathbb{Z} \rho \mathbb{Z}$  and, (iv) the SPAM noise channel followed by a Z error:  $\tilde{\mathcal{G}}_{\mathbb{Z}}(\rho) = f_q \mathbb{Z} \rho \mathbb{Z} + (1-f_q) \mathbb{Y} \rho \mathbb{Y}$ .

Solving the linear equation:

$$\mathcal{I} = \eta_0 \tilde{\mathcal{G}}_{\mathbb{I}} + \eta_1 \tilde{\mathcal{G}}_{\mathbb{X}} + \eta_2 \tilde{\mathcal{G}}_{\mathbb{Y}} + \eta_3 \tilde{\mathcal{G}}_{\mathbb{Z}} \quad (29)$$

we get the quasi-probability distribution as:  $\{|\eta_0|/\gamma_{\text{SPAM}}, |\eta_1|/\gamma_{\text{SPAM}}, 0, 0\}$  with

$$\begin{aligned} \eta_0 &= \frac{f_q}{2f_q - 1}, & \eta_1 &= -\frac{1-f_q}{2f_q - 1}, & \eta_2 &= \eta_3 = 0 \\ \text{sgn}(\eta_0) &= +1, & \text{sgn}(\eta_1) &= -1 \\ \gamma_{\text{SPAM}}(q) &= |\eta_0| + |\eta_1| \end{aligned} \quad (30)$$

Estimating  $f_q$  therefore provides a complete specification of the PEC coefficients.

3) *Composite noise in 5-qubit implementation of Bernstein-Vazirani algorithm*: The two noisy basis super-operators for each of the 5 distinct SPAM noise channels and the 16 noisy basis super-operators for the CNOT noise channel leads to 512 ( $16 \times 2^5$ ) noisy basis circuits  $\{\tilde{\mathcal{G}}_k\}$  for the 5-qubit Bernstein-Vazirani circuit, where  $k$  runs from 0 to 511.

Under the SPAM noise separability assumption,  $\gamma$  is obtained as:

$$\gamma = \gamma_{\text{CNOT}} \prod_{q=0}^4 \gamma_{\text{SPAM}}(q) \quad (31)$$

where  $\gamma_{SPAM}(q)$  refers to the  $\gamma_{SPAM}$  for the  $q$ -th qubit. The PEC coefficients for the Bernstein-Vazirani circuit are the elements of:

$$\{\eta_0^{\text{CNOT}}, \dots, \eta_{15}^{\text{CNOT}}\} \times \prod_{q=0}^4 \{\eta_0^{\text{SPAM}}(q), \eta_1^{\text{SPAM}}(q)\} \quad (32)$$

The quasi-probability distribution then follows as:  $\{\mathbb{Q}_k\} = \{|\eta_k^{\text{BV}}|/\gamma\}$ .

#### D. Adaptive noise model

In the context of our 5-qubit Bernstein-Vazirani setup, the noise parameters  $f_0$ ,  $f_1$ , and  $f_2$  are estimated using the method for uncorrelated parameters as they do not have CNOT correlations. The adaptive estimation of parameters  $f_3$ ,  $f_4$ ,  $x_C$ , and  $x_T$  employs the method for handling correlated parameters, detailed in Sec. III. The process is initiated within the Bayesian inference framework, which considers the probabilities of observing outcomes 00, 01, 10, and 11 on qubits 3 and 4, as depicted in Fig. 2, to be random variables. The estimation of the time-varying means and variances of these correlated noise parameters ( $f_3$ ,  $f_4$ ,  $x_C$ ,  $x_T$ ) is achieved by associating the mean values of the estimated densities directly with the parameters of the correlated noise model using:

$$\Pr(i) = \text{Tr} \left[ \Pi_i \mathcal{E}_4(\mathbb{L}_3 \mathcal{E}_2(\mathbb{L}_2 \mathbb{L}_1 \rho \mathbb{L}_1^\dagger \mathbb{L}_2^\dagger) \mathbb{L}_3^\dagger) \right] \quad (33)$$

where  $\Pi_i = |i\rangle\langle i|$  are the projection operators and  $i \in \{00, 01, 10, 11\}$ . For our running example, the probabilities are given by:

$$\begin{aligned} \Pr(00) &= f_3 f_4 (-1 - x_C x_T + x_C + x_T) \\ &\quad + f_3 (x_C x_T / 2 - x_T / 2) \\ &\quad + f_4 (1 - x_T - x_C / 2 + x_C x_T / 2) \\ &\quad - x_C x_T / 4 + x_T / 2 \\ \Pr(01) &= f_3 f_4 (1 - x_C - x_T + x_C x_T) \\ &\quad + f_3 (-1 - x_C x_T / 2 + x_C - x_T / 2) \\ &\quad + f_4 (-1 - x_C x_T / 2 + x_C + x_T) \\ &\quad + 1 + x_C x_T / 4 - x_C / 2 - x_T / 2 \\ \Pr(10) &= f_3 f_4 (1 - x_T - x_C + x_C x_T) \\ &\quad + f_3 (x_T / 2 - x_C x_T / 2) \\ &\quad + f_4 (x_C / 2 - x_C x_T / 2) \\ &\quad + x_C x_T / 4 \\ \Pr(11) &= f_3 f_4 (-1 + x_C + x_T - x_C x_T) \\ &\quad + f_3 (1 - x_T / 2 - x_C + x_C x_T / 2) \\ &\quad + f_4 (x_C x_T / 2 - x_C / 2) \\ &\quad + x_C / 2 - x_C x_T / 4 \end{aligned} \quad (34)$$

In the last step, the updated PEC coefficients are obtained using Eqn. 32.

#### E. Numerical simulation

For our 5-qubit circuit implementing the Bernstein-Vazirani algorithm, we used secret string  $r = 1000$ . Thus, the qubit-wise mean of the  $\mathbb{Z}$  observable for the noiseless case is given by:  $\langle \mathcal{O}_0 \rangle = +1$ ,  $\langle \mathcal{O}_1 \rangle = +1$ ,  $\langle \mathcal{O}_2 \rangle = +1$ ,  $\langle \mathcal{O}_3 \rangle = -1$ ,  $\langle \mathcal{O}_4 \rangle = +1$ , qubit 4 being the ancilla.

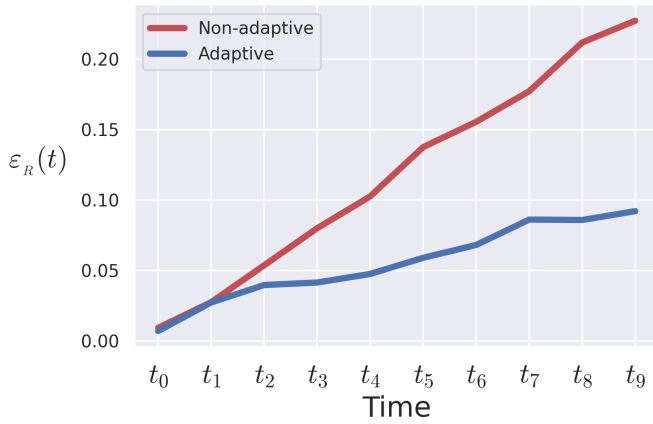
To validate our method, we used a numerical experiment that conducts a density matrix simulation of a 5-qubit noisy quantum circuit implementing the Bernstein-Vazirani algorithm using the Qiskit [56] software. The simulation begins with the mean of the beta distributions characterizing the SPAM fidelities for qubits 0-4 set at 0.96, 0.95, 0.94, 0.93, 0.92, respectively, and the mean of the depolarizing channel parameters for the control and target qubits in the CNOT gate both fixed at 0.017. Over the course of ten simulated time periods, the average SPAM fidelity for each qubit decreased by 0.01 per period, resulting in final mean SPAM fidelities of 0.86, 0.85, 0.84, 0.83, 0.82 for qubits 0-4, respectively. Similarly, the average depolarizing parameter for the CNOT gate also declined by 0.01 per time period, leading to a final mean value of 0.117 for both control and target qubits by the simulation's end. The noise parameters were adaptively estimated, per the methodology described in previous sections, using data generated by executing each of the 512 PEC circuits using 10,000 shots.

Fig. 4 demonstrates the simulated efficacy of the adaptive PEC algorithm. The plot compares the register accuracy and stability (averaged over the 5 qubits) achieved with the adaptive approach against a non-adaptive approach. It shows an improvement in accuracy of 59.5% in the final time period, when device noise is at its peak, with an average accuracy improvement of 53.4% across all ten periods. Similarly, stability improved by 58.0% in the last period, and by an average of 51.5% over the entire span of ten periods. The improvement in accuracy and stability of the outcomes from adaptive PEC occur due to more accurate noise characterizations using Bayesian inference.

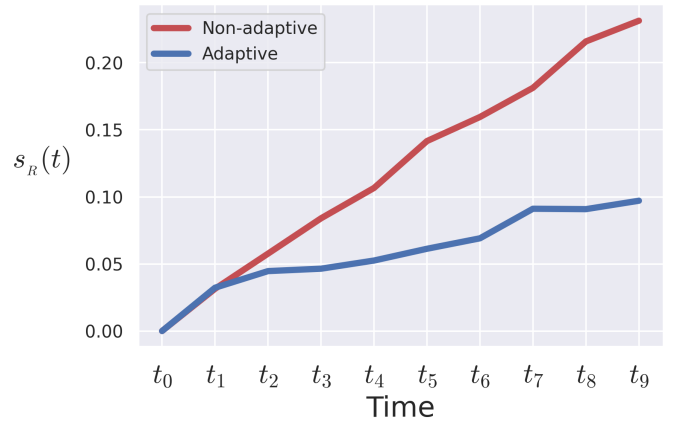
## V. EXPERIMENTAL TESTING

We tested the adaptive PEC method on the 27-qubit superconducting device called `ibm_kolkata`. Qubits 0,1,2,3,4 in Fig. 2 map to physical qubits 0,1,2,3,5 on the device shown in Fig. 5. The CNOT gate is between the physical qubits 3 (control) and 5 (target) on `ibm_kolkata`. Our dataset spans 24 hours and comprises 13 complete PEC datasets. It was collected on January 15, 2024, and have the following time-stamps: 00:01 hrs, 02:03 hrs, 03:50 hrs, 05:43 hrs, 07:23 hrs, 09:11 hrs, 10:53 hrs, 12:39 hrs, 14:22 hrs, 16:09 hrs, 17:50 hrs, 19:33 hrs, and 21:17 hrs. Each dataset is derived from measurements made in the computational basis, with each observation being a 5-bit string. The observations were obtained from the 512 noisy basis circuits, as described in Sec. IV-C, with each circuit repeated using  $L = 10,000$  shots, resulting in approximately 67 million observations in total.





(a)



(b)

**Figure 4:** Comparison of the adaptive PEC algorithm with a non-adaptive approach for a density matrix simulation that implements a noisy 5-qubit circuit for solving the Bernstein Vazirani problem. (a) Average accuracy across the 5-qubits and (b) Average stability across the 5-qubits.

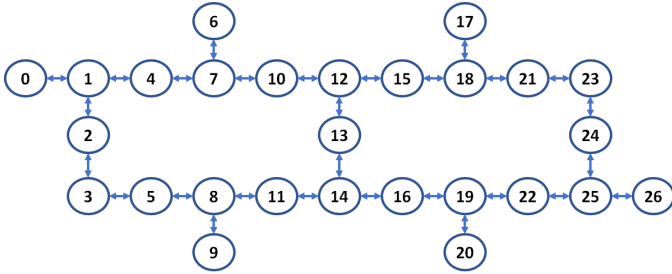


**Figure 5:** Qubit layout of the 27-qubit superconducting device `ibm_kolkata`. Circles represent superconducting transmons and lines indicate possible gate operations between sites.

### A. Non-stationary noise estimates

Fig. 6 illustrates how noise in the quantum computer changed over time. The blue line in plot (a) shows the depolarizing parameter for the target qubit of the CNOT gate, while the black line represents the depolarizing parameter for the control qubit. Plot (b) shows five lines, each representing the SPAM fidelity for the register elements. The x-axis denotes intra-calibration timestamps. The graph shows periods where the noise levels in the depolarizing parameter for qubit 3 (the control qubit) are steady, notably between 2:00 am and 7:30 am, contrasting with times of significant fluctuation, as observed between 9:00 am and 2:30 pm. The depolarizing parameter fluctuates between 1% and 4% for qubit 4 (the target qubit) and between 1% and 3% for qubit 3, both peaking sharply at 10:53 am.

Since the probabilities of observing the computational basis states on the left-hand side in Eqn. 33 are functions of time, we expect the SPAM fidelities to also vary over time. However, from Fig. 6 (b), the value for qubit 3 appears almost constant. This qubit exhibits less non-stationarity compared to other qubits, suggesting greater reliability with respect to

SPAM noise. However, these estimates are influenced by grid discretization used in the mean square error minimization procedure for solving the non-linear equations to find the best-fit. Our grid for SPAM fidelity had a spacing of 0.01 in the range  $[0, 1]$ . Our optimizer consistently produced an estimate for  $f_3$  as 0.99 across all the time-stamps, which is near the upper limit of the permissible range. We have not analyzed the impact of discretization granularity on degree of non-stationarity of the solution space.

Qubit 4 experiences the most significant impact from SPAM noise, with its values fluctuating between 0.99 and 0.94, a notable range given the sensitivity of PEC to accurate noise estimations. Meanwhile, Qubit 2 demonstrates a gradual drift in its values, starting from below 0.94 and rising to 0.96. This progressive change suggests a systematic, non-random trend that might be rectifiable with bias shift corrections. However, such patterns are not uniform across the entire register, implying the necessity to consider non-stationary statistics for modeling the system. Conducting experiments in times of significant non-stationary activity, like from 7:30 am to 2:30 pm, lead to more unstable outcomes when using non-adaptive PEC.

### B. Non-stationary quasi-probability distribution

Fig. 7 underscores the importance of considering the non-stationary nature of the quasi-probability distribution when implementing PEC, especially given the lengthy data collection process required for a single PEC mitigation (approximately 2 hours in our example). The abrupt change observed at 12:39 p.m. in the quasi-probability distribution directly correlates with the sharp change in the noise parameters characterizing the quantum circuit at the same time, as illustrated in Fig. 6.

To maintain clarity in Fig. 7, we have not plotted all 512 bins of the histogram in one plot. Fig. 7 (a) displays the time-varying weight  $Q_0$  for the Bernstein-Vazirani circuit as-is without any

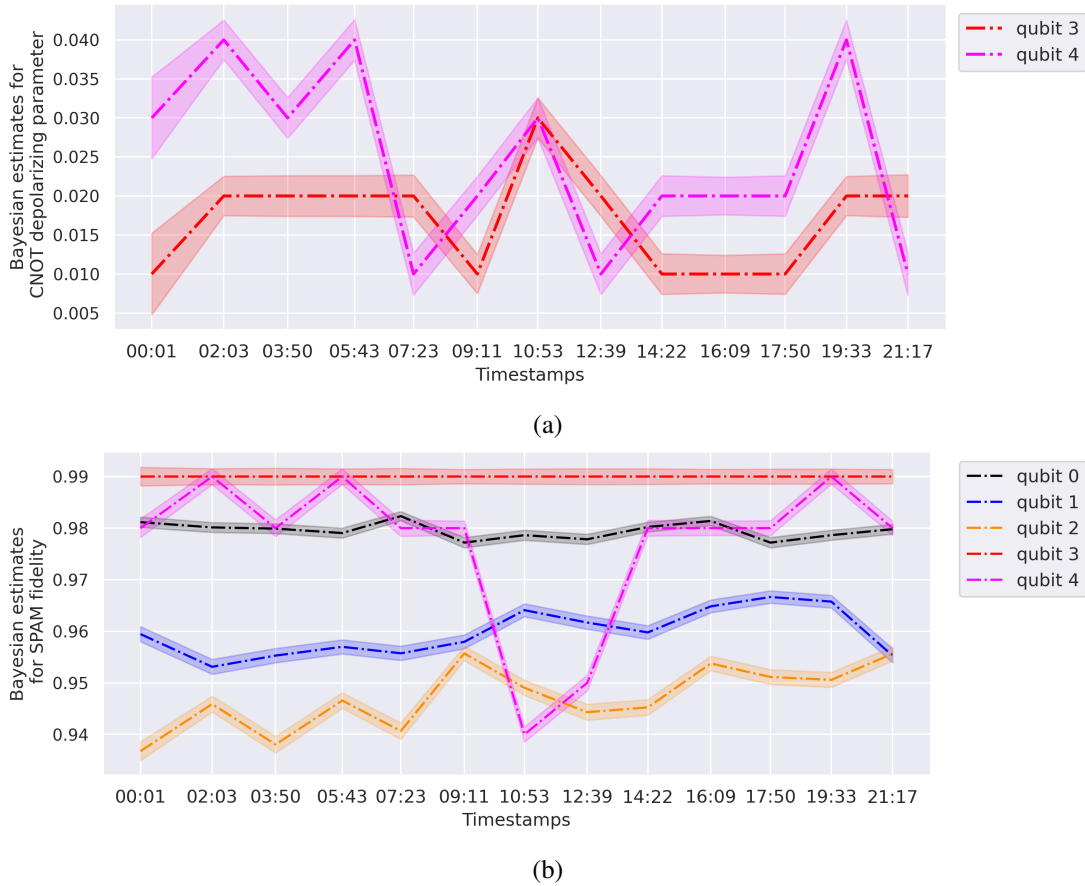


**Figure 6:** This figure depicts the non-stationary noise on the experimental device `ibm_kolkata`. In plot (a), the blue line represents the depolarizing parameter for the target qubit, while the black line denotes the depolarizing parameter for the control qubit in the CNOT gate. Plot (b) illustrates five lines, each indicating the SPAM fidelity for the register elements. The x-axis corresponds to intra-calibration timestamps for January 15. The shaded regions denote the time-varying standard deviations.

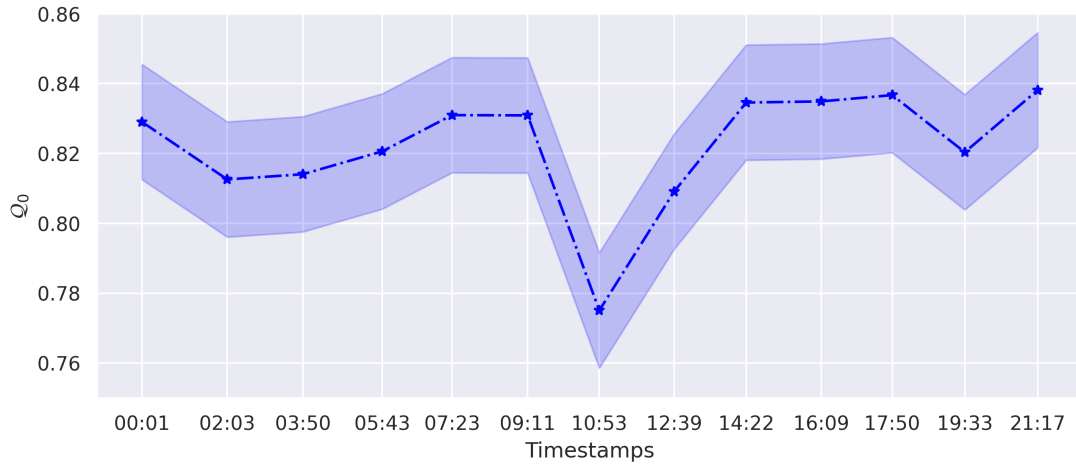
additional Pauli-gate added (we also refer to this as the raw Bernstein-Vazirani circuit). If the circuit were noiseless, then the weight for the raw circuit will be a constant 1. We observe a decrease in weight for the raw circuit, dipping below 78% around 10:53 am from a peak of almost 83%, coinciding with a peak in circuit noise as seen in Fig. 6. This decrease in weight is expected as the circuit noise peaks.

The values of the quasi-probability bins for the next 10 basis circuits are shown in plot (b), with values approximately 10 times lower than the first circuit. Ignoring seemingly small coefficients in the quasi-probability distribution without considering the precision of final reported results can be risky. Subsequent basis circuits, not shown here, have significantly smaller quasi-probability weights (around  $10^{-4}$ ). Yet their collective impact in a sum of 500 can be substantial, contributing up to 0.05. Given our reported accuracy and stability are around  $10^{-2}$ , these coefficients, though small, can significantly influence the results. Therefore, in our analysis, we included all basis circuits without approximation, focusing on the effects of non-stationary noise on PEC, rather than on resource optimization.

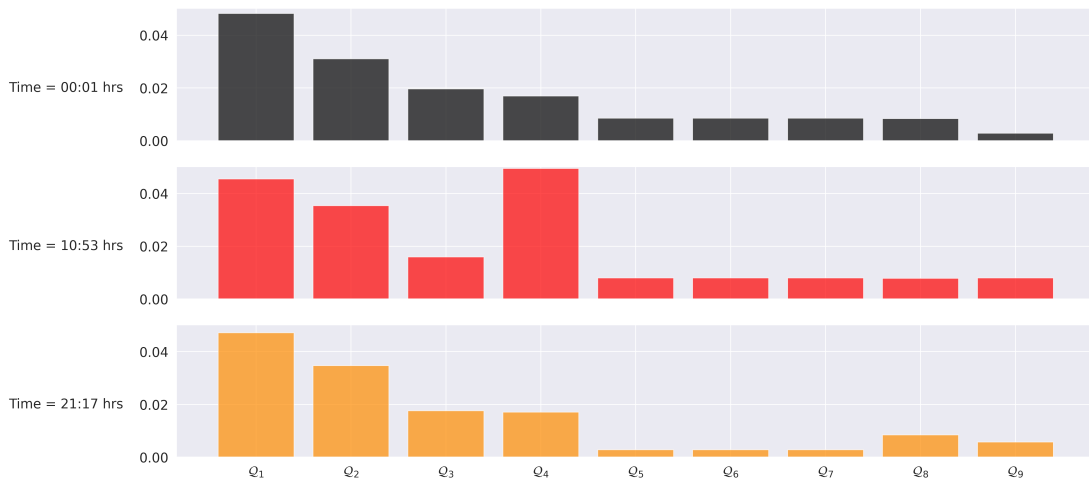
### C. Non-stationary PEC outcomes

The impact of the non-stationary noise can be seen in Fig. 8. The first plot, labeled No mitigation, presents the accuracy and stability metrics defined in Eqns. 20 and 23 respectively, for the raw Bernstein Vazirani circuit without any form of quantum error mitigation. The second plot, labeled ROEM, which stands for readout error mitigation, displays the metrics after performing SPAM noise mitigation. In this case, the SPAM noise parameters are held constant after initial device characterization. It deploys the standard matrix inversion [45] technique for mitigation. The third plot, labeled non-adaptive PEC, exhibits the accuracy and stability metrics for the Bernstein Vazirani circuit with non-adaptive PEC. This method incorporates SPAM noise mitigation within the PEC framework, as detailed in Sec. IV-C. The fourth plot, labeled adaptive PEC, presents the metrics for the adaptive PEC method, as discussed in Sec. III.

Fig. 8 (a) shows the effectiveness of the adaptive PEC in enhancing result accuracy. It reveals approximately a 42% improvement in accuracy on average compared to the non-



(a)



(b)

**Figure 7:** These plots depict the non-stationary nature of the quasi-probability distribution. To maintain clarity, we opted not to plot all 512 bins of the histogram in a single plot. In (a), we observe the time-varying weight  $Q_0$  for the raw Bernstein-Vazirani circuit which carries the most substantial weight, accounting for almost 80% of the distribution. In (b), we show the values of the quasi-probability bins for the subsequent 10 basis circuits, which are more than 10 times lower in magnitude compared to the first circuit. The non-stationary nature of the quasi-probability distribution becomes crucial given the lengthy data collection process required for PEC mitigation because the noise estimation becomes inaccurate in these time-frames. Our experiment took approximately 2 hours for each dataset comprising 512 circuits.

adaptive method. The observed accuracy benefit ranges from a minimum of 25% to a maximum of 78%. Fig. 8 (b) shows the impact on result stabilization. It shows an approximately 60% enhancement in stability on average compared to the non-adaptive method. The observed stability benefit ranges from a minimum of 8% to a maximum of 200%.

Observing the plots, it is evident that adaptive PEC significantly outperforms standard PEC. Additionally, all four methods (no mitigation, ROEM, PEC, and adaptive PEC) exhibit a time-series trend that deteriorates notably at 10:53 am. The observation correlates with the abrupt change in the underlying quasi-probability distribution at 10:53 am as seen in Fig. 7.

Both the accuracy and stability metrics at 12:39 p.m. are slightly worse for adaptive PEC compared to non-adaptive PEC. This discrepancy stands out as the only instance where adaptive PEC performs sub-optimally. It seems, surprisingly, that the stale data serves as a better noise estimate for this specific time-point. However, the noise at 12:39 p.m. is not necessarily closer to the noise at the starting time-stamp of 00:01 a.m., as demonstrated in Fig. 6. While adaptive PEC succeeds in most cases, the learning process is not instantaneous. There exists a slight lag in learning due to the influence of prior information on the final estimate. This phenomenon reflects a fundamental aspect of learning methods: the presence of memory, which can aid learning but also slows down adaptation

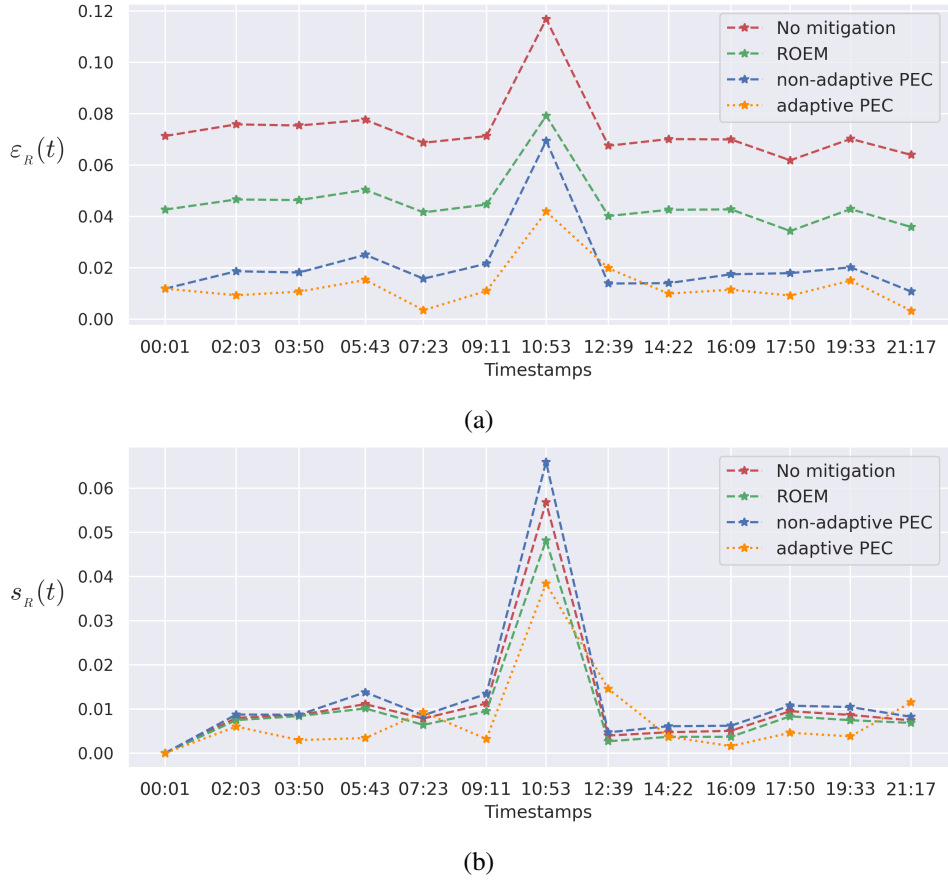


**Figure 8:** The figure comprises two plots, each depicting four graphs: (1) "No mitigation" presents raw Bernstein-Vazirani metrics without error mitigation, (2) "ROEM" shows metrics after readout error mitigation, with constant SPAM noise parameters, (3) "Non-adaptive PEC" displays metrics for PEC, and (4) "Adaptive PEC" exhibits metrics for PEC with adaptive noise mitigation. The x-axis denotes intra-calibration time-stamps (UTC) for Jan 15. Plot (a) illustrates the time-varying accuracy metric from Eqn. 20. It demonstrates the adaptive PEC's 42% accuracy improvement over non-adaptive PEC. Plot (b) shows the time-varying stability metric from Eqn. 23. It illustrates the adaptive PEC's 60% stability enhancement compared to non-adaptive PEC. These plots underscore the significant impact of non-stationary noise on PEC resilience. Due to PEC's lengthy completion time (a couple of hours), adaptive methods are able to handle non-stationary noise conditions better.

to the fast, spiky changes. The sharp change in noise at 10:53 a.m. leads to an overestimation of the noise estimate compared to when using the initial value at 00:01 a.m. as a reference point. Residual errors in the noise estimates likely arises from inaccurate models and non-stationary processes changing at a faster rate than sampled here.

## VI. CONCLUSION

Characterizing noise in contemporary quantum devices remains challenging due to their non-stationary statistics [22], rendering mitigation strategies [18] highly susceptible to errors arising from statistical estimation. Incorrect assumptions, such as neglecting non-stationarity, can yield misleading and irreproducible results.

This study examined the impact of non-stationary noise on probabilistic error cancellation (PEC). It introduced a Bayesian approach to improve stability and accuracy of PEC outcomes.

We tested our algorithm on the `ibm_kolkata` device on January 15, 2024. The dataset covered a 24-hour period, consisting of 13 complete PEC datasets for the Bernstein-Vazirani test circuit, with approximately 67 million observations. Results indicate a 42% increase in accuracy and a 60% enhancement in stability compared to non-adaptive PEC. Consistent improvement trends across time-stamps and qubits provide robust evidence for the effectiveness of adaptive PEC.

The choice of noise model influences the estimation process. If the chosen noise model is incorrect or insufficiently granular, the estimated noise parameters will reflect the specific dataset's inherent patterns rather than accurately representing a true noise model applicable for various inputs. Mitigation using such mis-estimated noise models will be unsuccessful because the mitigation algorithm will introduce additional errors to the already noisy data. Improvements in mitigation results, including improved performance vs non-adaptive PEC shown



here, indicate that the noise is sufficiently well-characterized using our simplified noise model but additional improvements on accuracy and stability can be obtained by using more frequent adaptive estimates.

Our goal in this paper was not to provide examples of performing Bayesian inference in different quantum computing contexts. Instead, we aimed to highlight that non-stationary noise is a significant issue in contemporary quantum computers, necessitating adaptive methods. Bayesian inference represents one such method. While our framework is generic, the specific equations for inference will differ based on the application. We illustrated our methodology using Bernstein-Vazirani as a test case for improving probabilistic error cancellation in presence of non-stationary noise.

Before concluding, we will discuss the scalability of the proposed algorithm. There are three potential areas where scalability may be a concern: PEC resource costs, optimization costs, and sampling costs.

A) PEC resource costs: The first scalability concern pertains to the number of PEC circuits required and is not directly related to Bayesian inference. The problem is well-known: each CNOT gate requires 16 PEC circuits for mitigating CNOT noise, and each qubit needs 2 PEC circuits for SPAM noise mitigation. Consequently, a Bernstein-Vazirani circuit with  $m$  CNOT gates and  $n$  qubits will need  $2^{4m+n}$  PEC circuits. To mitigate this, one strategy is to avoid using PEC for SPAM mitigation and instead use standard matrix inversion (which may compromise some accuracy). Additionally, noise can be modeled in modular circuit layers, with PEC applied to these modules (instead of individual quantum gates).

B) Optimization: The second concern involves solving the non-linear system of equations (cf. Eqns. 34). In the Bernstein-Vazirani circuit, with  $n$  qubits and  $m$  CNOT gates, there are  $2m + n$  noise parameters: each qubit contributes one SPAM parameter, and each CNOT gate's asymmetric depolarizing noise model contributes  $2m$  parameters. For an  $n$ -qubit problem, there can be  $2^n$  such equations, one for each computational basis state. When  $2m + n < 2^n$ , we have an over-determined system that can be solved using mean square error minimization. However, this is computationally expensive due to the high-dimensional search space for correlated parameters. If the system is under-determined, the estimates are unreliable due to multiple possible solutions. To make the algorithm scalable, focus on the most significant sources of noise and avoid overly detailed models that do not contribute significantly to noise explanation. For example, in this paper, we ignored gate noise in single-qubit gates and focused on SPAM noise and noise in entangling gates. In fact, even with quantum error correction, statistical mitigation methods may be relevant due to unforeseen noise sources. A single logical qubit may consist of thousands of physical qubits, so it is crucial to model noise at an aggregate, modular level (e.g., the logical level) rather than at lower levels of the

computing stack. Choosing the right level of abstraction and avoiding overly granular noise models reduces the number of noise parameters that need to be estimated.

C) Sampling: Parameter estimation using Bayesian inference often requires sampling from a multivariate correlated distribution. However, the algorithm presented in this paper for estimating time-varying circuit noise parameters eliminates the need for sampling. As demonstrated in Eqn. 10, the parameters of the Dirichlet distribution, which models the joint density for the probability simplex, are updated using observed data  $\mathcal{D}$ , which help us formulate the system of non-linear equations to estimate the time-varying noise parameters. However, if custom metrics such as 95% confidence intervals are needed, or if we prefer using the maximum-a-posteriori (MAP) estimate instead of the mean, then Monte Carlo sampling will be required, which has a high computational overhead.

#### CODE AND DATA

The code and data are for available publicly available in the github repository: <https://github.com/quantumcomputing-lab/pecTVQN/>

#### ACKNOWLEDGMENTS

This material is based upon work supported by the US Department of Energy, Office of Science, National Quantum Information Science Research Centers, Quantum Science Center.

#### REFERENCES

- [1] Travis S Humble, Himanshu Thapliyal, Edgard Munoz-Coreas, Fahd A Mohiyaddin, and Ryan S Bennink. Quantum computing circuits and devices. *IEEE Design & Test*, 36(3):69–94, 2019.
- [2] Antoine Browaeys and Thierry Lahaye. Many-body physics with individually controlled rydberg atoms. *Nature Physics*, 16(2):132–142, 2020.
- [3] Ashley Montanaro. Quantum algorithms: an overview. *npj Quantum Information*, 2(1):1–8, 2016.
- [4] Jiangwei Shang, Yi-Lin Seah, Hui Khoon Ng, David John Nott, and Berthold-Georg Englert. Monte carlo sampling from the quantum state space. i. *New Journal of Physics*, 17(4):043017, 2015.
- [5] Giovanni Espitia. On the role of quantum computing in science and cybersecurity. *arXiv:2105.09942*, 2021.
- [6] Meng-Leong How and Sin-Mei Cheah. Business renaissance: Opportunities and challenges at the dawn of the quantum computing era. *Businesses*, 3(4):585–605, 2023.
- [7] Quantum roadmap. Available online: <https://www.ibm.com/roadmaps/quantum/> (accessed on 12 feb 2024).

- [8] Thomas E Roth, Ruichao Ma, and Weng C Chew. An introduction to the transmon qubit for electromagnetic engineers. *arXiv:2106.11352*, 2021.
- [9] John Preskill. Quantum computing in the nisq era and beyond. *Bulletin of the American Physical Society*, 64, 2019.
- [10] Abhinav Kandala, Kristan Temme, Antonio D Córcoles, Antonio Mezzacapo, Jerry M Chow, and Jay M Gambetta. Error mitigation extends the computational reach of a noisy quantum processor. *Nature*, 567(7749):491–495, 2019.
- [11] Pedro Parrado-Rodríguez, Ciarán Ryan-Anderson, Alejandro Bermudez, and Markus Müller. Crosstalk suppression for fault-tolerant quantum error correction with trapped ions. *Quantum*, 5:487, 2021.
- [12] Chao Fang, Ye Wang, Shilin Huang, Kenneth R Brown, and Jungsang Kim. Crosstalk suppression in individually addressed two-qubit gates in a trapped-ion quantum computer. *Physical Review Letters*, 129(24):240504, 2022.
- [13] Suhas Vittal, Poulami Das, and Moinuddin Qureshi. Eraser: Towards adaptive leakage suppression for fault-tolerant quantum computing. In *Proceedings of the 56th Annual IEEE/ACM International Symposium on Microarchitecture*, pages 509–525, 2023.
- [14] Martin Kliesch and Ingo Roth. Theory of quantum system certification. *PRX Quantum*, 2(1):010201, 2021.
- [15] G.A.L. White, F.A. Pollock, L.C.L. Hollenberg, K. Modi, and C.D. Hill. Non-markovian quantum process tomography. *PRX Quantum*, 3:020344, May 2022.
- [16] Robin J Blume-Kohout. Modeling and characterizing noise in quantum processors. Technical report, Sandia National Lab.(SNL-NM), Albuquerque, NM (United States), 2020.
- [17] Robin Blume-Kohout. Optimal, reliable estimation of quantum states. *New Journal of Physics*, 12(4):043034, 2010.
- [18] Kishor Bharti, Alba Cervera-Lierta, Thi Ha Kyaw, Tobias Haug, Sumner Alperin-Lea, Abhinav Anand, Matthias Degroote, Hermann Heimonen, Jakob S Kottmann, Tim Menke, et al. Noisy intermediate-scale quantum algorithms. *Reviews of Modern Physics*, 94(1):015004, 2022.
- [19] Samuele Ferracin, Seth T Merkel, David McKay, and Animesh Datta. Experimental accreditation of outputs of noisy quantum computers. *arXiv:2103.06603*, 2021.
- [20] Ted Thorbeck, Andrew Eddins, Isaac Lauer, Douglas T McClure, and Malcolm Carroll. Two-level-system dynamics in a superconducting qubit due to background ionizing radiation. *PRX Quantum*, 4(2):020356, 2023.
- [21] Matt McEwen, Lara Faoro, Kunal Arya, Andrew Dunsworth, Trent Huang, Seon Kim, Brian Burkett, Austin Fowler, Frank Arute, Joseph C Bardin, et al. Resolving catastrophic error bursts from cosmic rays in large arrays of superconducting qubits. *Nature Physics*, 18(1):107–111, 2022.
- [22] Josu Etxezarreta Martinez, Patricio Fuentes, Pedro Crespo, and Javier Garcia-Frias. Time-varying quantum channel models for superconducting qubits. *npj Quantum Information*, 7(1):1–10, 2021.
- [23] Clemens Müller, Jürgen Lisenfeld, Alexander Shnirman, and Stefano Poletto. Interacting two-level defects as sources of fluctuating high-frequency noise in superconducting circuits. *Physical Review B*, 92(3):035442, 2015.
- [24] PV Klimov, Julian Kelly, Z Chen, Matthew Neeley, Anthony Megrant, Brian Burkett, Rami Barends, Kunal Arya, Ben Chiaro, Yu Chen, et al. Fluctuations of energy-relaxation times in superconducting qubits. *Physical Review Letters*, 121(9):090502, 2018.
- [25] John M Martinis. Qubit metrology for building a fault-tolerant quantum computer. *npj Quantum Information*, 1(1):1–3, 2015.
- [26] Samudra Dasgupta and Travis S. Humble. Impact of unreliable devices on stability of quantum computations. *arxiv: 2307.06833*, 2024.
- [27] Samudra Dasgupta and Travis S Humble. Stability of noisy quantum computing devices. *arXiv:2105.09472*, 2021.
- [28] Samudra Dasgupta and Travis S Humble. Characterizing the stability of NISQ devices. In *2020 IEEE International Conference on Quantum Computing and Engineering*, pages 419–429. IEEE, 2020.
- [29] Malcolm Carroll, Sami Rosenblatt, Petar Jurcevic, Isaac Lauer, and Abhinav Kandala. Dynamics of superconducting qubit relaxation times. *arXiv:2105.15201*, 2021.
- [30] Corey Rae H McRae, Gregory M Stiehl, Haozhi Wang, Sheng-Xiang Lin, Shane A Caldwell, David P Pappas, Josh Mutus, and Joshua Combes. Reproducible coherence characterization of superconducting quantum devices. *Applied Physics Letters*, 119(10):100501, 2021.
- [31] Qian Xu, Alireza Seif, Haoxiong Yan, Nam Mannucci, Bernard Ousmane Sane, Rodney Van Meter, Andrew N Cleland, and Liang Jiang. Distributed quantum error correction for chip-level catastrophic errors. *Physical Review Letters*, 129(24):240502, 2022.
- [32] Timothy Proctor, Melissa Revelle, Erik Nielsen, Kenneth Rudinger, Daniel Lobser, Peter Maunz, Robin Blume-Kohout, and Kevin Young. Detecting and tracking drift in quantum information processors. *Nature Communications*, 11(1):1–9, 2020.

- [33] Arshag Danageozian, Ashe Miller, Pratik J Barge, Narayan Bhusal, and Jonathan P Dowling. Noisy coherent population trapping: applications to noise estimation and qubit state preparation. *Journal of Physics B: Atomic, Molecular and Optical Physics*, 55(15):155503, 2022.
- [34] Swarnadeep Majumder, Leonardo Andreta de Castro, and Kenneth R Brown. Real-time calibration with spectator qubits. *npj Quantum Information*, 6(1):19, 2020.
- [35] Youngseok Kim, Luke CG Govia, Andrew Dane, Ewout van den Berg, David M Zajac, Bradley Mitchell, Yinyu Liu, Karthik Balakrishnan, George Keefe, Adam Stabile, et al. Error mitigation with stabilized noise in superconducting quantum processors. *arXiv preprint arXiv:2407.02467*, 2024.
- [36] Ivan Henao, Jader P Santos, and Raam Uzdin. Adaptive quantum error mitigation using pulse-based inverse evolutions. *npj Quantum Information*, 9(1):120, 2023.
- [37] Michael A Nielsen and Isaac Chuang. Quantum computation and quantum information, 2002.
- [38] Kristan Temme, Sergey Bravyi, and Jay M Gambetta. Error mitigation for short-depth quantum circuits. *Physical Review Letters*, 119(18):180509, 2017.
- [39] Giacomo Torlai, Christopher J Wood, Atithi Acharya, Giuseppe Carleo, Juan Carrasquilla, and Leandro Aolita. Quantum process tomography with unsupervised learning and tensor networks. *arXiv:2006.02424*, 2020.
- [40] Ewout Van Den Berg, Zlatko K Mineev, Abhinav Kandala, and Kristan Temme. Probabilistic error cancellation with sparse pauli-lindblad models on noisy quantum processors. *Nature Physics*, pages 1–6, 2023.
- [41] Youngseok Kim, Andrew Eddins, Sajant Anand, Ken Xuan Wei, Ewout Van Den Berg, Sami Rosenblatt, Hasan Nayfeh, Yantao Wu, Michael Zaletel, Kristan Temme, et al. Evidence for the utility of quantum computing before fault tolerance. *Nature*, 618(7965):500–505, 2023.
- [42] Ethan Bernstein and Umesh Vazirani. Quantum complexity theory. In *Proceedings of the twenty-fifth annual ACM symposium on theory of computing*, pages 11–20, 1993.
- [43] Joseph M Lukens, Kody JH Law, Ajay Jasra, and Pavel Lougovski. A practical and efficient approach for bayesian quantum state estimation. *New Journal of Physics*, 22(6):063038, 2020.
- [44] Muqing Zheng, Ang Li, Tamás Terlaky, and Xiu Yang. A bayesian approach for characterizing and mitigating gate and measurement errors. *arXiv:2010.09188*, 2020.
- [45] Sergey Bravyi, Sarah Sheldon, Abhinav Kandala, David C Mckay, and Jay M Gambetta. Mitigating measurement errors in multiqubit experiments. *Physical Review A*, 103(4):042605, 2021.
- [46] Quasi-probability representation of an ideal gate. Available online: <https://mitiq.readthedocs.io/en/v0.11.1/examples/pec-tutorial.html#task-2-sampling-from-the-quasi-probability-representation-of-an-ideal-gate/> (last accessed on 25 mar 2024).
- [47] Jonathan J Burnett, Andreas Bengtsson, Marco Scigliuzzo, David Niepce, Marina Kudra, Per Delsing, and Jonas Bylander. Decoherence benchmarking of superconducting qubits. *npj Quantum Information*, 5(1):1–8, 2019.
- [48] Neil J Gordon, David J Salmond, and Adrian FM Smith. Novel approach to nonlinear/non-gaussian bayesian state estimation. In *IEE Proceedings F-radar and Signal Processing*, volume 140, pages 107–113. IET, 1993.
- [49] Jayesh H Kotecha and Petar M Djuric. Gaussian sum particle filtering. *IEEE Transactions on Signal Processing*, 51(10):2602–2612, 2003.
- [50] Andrew Gelman, John B Carlin, Hal S Stern, and Donald B Rubin. *Bayesian data analysis*. Chapman and Hall/CRC, 1995.
- [51] Devinderjit Sivia and John Skilling. *Data analysis: a Bayesian tutorial*. OUP Oxford, 2006.
- [52] Christian P Robert, George Casella, and George Casella. *Introducing monte carlo methods with r*, volume 18. Springer, 2010.
- [53] Peter M Lee. *Bayesian statistics*. Oxford University Press London:, 1989.
- [54] David C McKay, Christopher J Wood, Sarah Sheldon, Jerry M Chow, and Jay M Gambetta. Efficient z gates for quantum computing. *Physical Review A*, 96(2):022330, 2017.
- [55] Alistair WR Smith, Kiran E Khosla, Chris N Self, and MS Kim. Qubit readout error mitigation with bit-flip averaging. *Science Advances*, 7(47):eabi8009, 2021.
- [56] Thomas Alexander, Naoki Kanazawa, Daniel J Egger, Lauren Capelluto, Christopher J Wood, Ali Javadi-Abhari, and David C McKay. Qiskit pulse: programming quantum computers through the cloud with pulses. *Quantum Science and Technology*, 5(4):044006, 2020.